Title	Influence of Different Dissolved Gases on Electrocatalytic Nitrate Sensing Performance at Cu- modified Au Electrode			
Author(s)	Islam, Motasim B.; Hossain, Mohammad Imran; Hosen, Nazmul; Rahaman, Mostafizur; Singha, Nayan Ranjan; Aoki, Kentaro; Nagao, Yuki; Hasnat, Mohammad A.			
Citation	ChemistrySelect, 9(36): e202402986			
Issue Date	2024-09-23			
Туре	Journal Article			
Text version	author			
URL	http://hdl.handle.net/10119/20020			
Rights	This is the peer reviewed version of the following article: M. B. Islam, M. I. Hossain, N. Hosen, M. Rahaman, N. R. Singha, K. Aoki, Y. Nagao, M. A. Hasnat, ChemistrySelect 2024, 9, e202402986, which has been published in final form at https://doi.org/10.1002/slct.202402986. This article may be used for non-commercial purposes in accordance with Wiley Terms and Conditions for Use of Self-Archived Versions. This article may not be enhanced, enriched or otherwise transformed into a derivative work, without express permission from Wiley or by statutory rights under applicable legislation. Copyright notices must not be removed, obscured or modified. The article must be linked to Wiley's version of record on Wiley Online Library and any embedding, framing or otherwise making available the article or pages thereof by third parties from platforms, services and websites other than Wiley Online Library must be prohibited.			
D				
Description	TAIST —			

JAPAN ADVANCED INSTITUTE OF SCIENCE AND TECHNOLOGY

Influence of Different Dissolved Gases on Electrocatalytic Nitrate Sensing Performance at Cu-modified Au Electrode

Motasim B. Islam^a, Mohammad Imran Hossain^a, Nazmul Hosen^b, Mostafizur Rahaman^c, Nayan Ranjan Singha^d, Kentaro Aoki^e, Yuki Nagao^e, Mohammad A. Hasnat^{a,f,*}

^a Electrochemistry & Catalysis Research Laboratory (ECRL), Department of Chemistry, School of Physical Sciences, Shahjalal University of Science and Technology, Sylhet-3114, Bangladesh

^b Department of Chemistry and Biochemistry, The University of Southern Mississippi, Hattiesburg, MS 39406, USA

^c Department of Chemistry, College of Science, King Saud University, P.O. Box 2455, Riyadh 11451, Saudi Arabia

^dAdvanced Polymer Laboratory, Department of Polymer Science and Technology, Government College of Engineering and Leather Technology (Post-Graduate), Kolkata-700106, West Bengal, India

^e School of Materials Science, Japan Advanced Institute of Science and Technology, 1-1 Asahidai, Nomi, Ishikawa 923-1292, Japan

^f International Research Organization for Advanced Science and Technology (IROAST), Kumamoto University, Kumamoto 860-8555, Japan

Corresponding author: M. A. Hasnat (mah-che@sust.edu)

Abstract

The present study investigates the electrocatalytic nitrate reduction reaction (NRR) on a Cu/Au electrode surface in a neutral pH potassium chloride (KCl) environment saturated with nitrogen, oxygen, and carbon dioxide, three of the most abundant atmospheric gases. The electrode was characterized using OCP, EIS, SEM, EDX, XPS, and XRD to assess its electrochemical properties, catalytic feasibility, and surface morphology. Results indicated that nitrate ions undergo a

consecutive reduction process $(NO_3^- \to NO_2^- \to NH_3)$ on the Cu/Au electrode. O₂ saturated environment impeded the NRR process through O₂ adsorption on the electrode surface prior to the $NO_3^- \to NO_2^-$ conversion. In contrast, CO₂ saturated condition enhanced the reaction by neutralizing the NRR byproduct OH^- ions, thus accelerating the overall NRR kinetics. Under CO₂ environment the NRR process was found more facile compared to that of other two gases. NRR took place at a peak potential of -0.71 V and -1.06 V for the first and second reduction wave, respectively. Kinetic analysis showed that the reduction reactions in presence of CO₂ followed first-order, diffusion-limited kinetics. The Cu/Au electrode exhibited high sensitivity $(3.49 \times 10^{-1} \, \mu A \, \mu M^{-1})$ with an LOD of 0.46 μM for nitrate detection, and finally demonstrated excellent performance in real sample analysis.

Introduction

One of the modern world's major concerns is groundwater contamination by different harmful ions.[1-4] One significant anion contamination is caused by nitrate due to industrialization, agricultural means, improper waste disposal, urbanization, and natural processes. [2] The non-point source of nitrate contamination can be from animal manure to septic tanks, depending on the different geographical location. [5] Besides the nitrate ion (NO_3^-) , other nitrogen-containing common ions present in water bodies are nitrite (NO_2^-) and ammonium (NH_4^+) .^[6] The decomposition of organic waste can initiate ammonia production in the nitrogen cycle of a water body.^[7] Fish respiration produces ammonia and ammonium too.^[8] Ammonium can be oxidized and turn into nitrate after a two-step reaction by aerobic microorganisms.^[9] These chemoautotrophic bacteria, i.e., Nitrobacter and Nitrosomonas bacteria, can function under near-zero dissolved oxygen levels.^[10,11] However, it is expected that the nitrogen cycle would balance the production of ammonium in water bodies, which does, but the excessive contamination by both point and nonpoint sources imbalance it.[12] A significant number of findings by the researchers worldwide revealed an imbalance in the natural nitrogen cycle that might be attributed to the expanded availability and application of nitrogen-containing chemicals to feed an increased population during the last several decades.^[12–16] Besides the degradation of organic materials, nitrogen from inorganic sources can trouble the aquatic ecosystem through anthropogenic sources, for example, industrial debris, agribusiness, sewage effluents, and metropolitan and farming run-off. [16-21] Eutrophication resulting from such disruption severely threatens both nature and humans. Agriculture causes eutrophication, but we cannot eliminate it as it is crucial for nutrition needs. [22,23] Fertilizer leaching from agro-farms pollutes the groundwater and soil. Determining the nitrate content in groundwater is becoming increasingly crucial as increased nitrate contamination increases health risks.

The health outcomes of drinking water with high nitrate levels might be detrimental. To avoid potential risks, it is best to ensure that our water is within acceptable nitrate levels. The maximum level of nitrate allowed in water is set by the US Environmental Protection Agency (EPA) to ensure that it is safe for consumption. They set the maximum contaminant level (MCL) for nitrate in water as ten ppm (parts per million) or 10 mg/L as (NO_3^-N), 50 ppm as NO3, and 0.5 ppm as NH3. The World Health Organization (WHO) and European directives law have also established a similar MCL value for nitrate in water.^[24] Monitoring the nitrate levels in drinking water is essential to ensure they do not exceed these safe levels. For example, it can impose harmful impacts, particularly for infants and pregnant women. The infant has been found to get methemoglobinemia at a lower concentration than 50 ppm nitrate. The MCL for infants is set as ten ppm nitrate and one ppm nitrite.^[25,26] Besides, methemoglobinemia in infants, congenital disabilities, cancer formation (breast, bladder, and colorectal), liver damage, and thyroid disease are caused by nitrate contamination.^[27,28] Due to these fatal consequences, the demand for monitoring nitrate contamination in daily drinking water, food industries, and wastewater has been increasing gradually.^[29-31]

There are many ways to analyze nitrate levels these days.^[32] The techniques include ion exchange chromatography,^[33,34] colorimetry,^[35,36] polarography,^[37] and UV spectroscopy.^[38]Despite each procedure having benefits, they are all dependent on specialized tools and skilled operators, which can be strenuous and inconsistent in terms of lacking selectivity and sensitivity. It is vital to continuously monitor biological denitrification processes for effective nitrate reduction reaction (NRR) by controlling pH levels, adding a carbon source, and maintaining appropriate temperatures.^[32,39] Heterogeneous catalysis is another option. Still, it can also result in secondary

pollution and may be relatively expensive. [40] Bimetallic electrodes have been the subject of research efforts to handle product selectivity and enhance reduction behavior. [41-43] Researchers have accomplished this by utilizing metal alloys and copper-based films on the exterior of a core metal. This is an excellent way to address the concerns with extractive techniques like ion exchange resins and reverse osmosis. These methods can sometimes cause secondary pollution, which needs to be treated, ultimately adding to the overall cost of the process. Researchers have put effort into inventing cost-effective techniques for nitrate reduction. Electrochemical techniques are employed to explore different catalytic metals to reduce nitrate effectively. Earth-abundant metals (Fe, Co, Ni, Cu) and precious metals (Pt, Ir) have been studied, and the Cu-made electrochemical electrodes show efficient catalytic behavior towards nitrate reduction reactions. [44,45] Recently, it has been reported that Pt is an excellent support for Cu particles to detect nitrate ions from the aqueous systems.^[46–48] However, the inherent reduction of Cu(I/II) species competes with nitrate reduction over the Cu/Pt surface as the oxide to nitrate reduction peak separation is only 0.21 V. Additionally, often the hydrogen evolution reaction (HER) by water splitting competes with NRR over the Pt-based electrode surfaces, declining the electrode's efficiency. [49,50] These facts make a Pt-based surface critical for developing an interference-free electrochemical sensor, primarily via reduction reactions.

Therefore, alternative support for copper particles in developing a nitrate sensor is imperative. Since gold is highly resistant to corrosion and has an extended potential window about HER, [51,52] a gold surface may be a good alternative for developing a nitrate sensor. Literature have documented that the modification of a gold surface with copper facilitates NRR in acidic condition. [53] However, in acidic condition, copper-based materials exhibit instability and susceptibility to corrosion on electrode surfaces. [54,55] In this research, for the first time, we have explored the potential of using a Cu/Au surface as a nitrate sensor via electrocatalytic reduction reactions in a neutral medium. This approach more accurately mimics the pH of natural water sources and includes the presence of commonly occurring dissolved gases such as N2, O2, and CO2. Researchers often degas the experimental solution by purging molecular nitrogen to nullify the impacts of dissolved O2 gas, as O2 reduction signals may interfere with signals of target reactions. However, rarely one investigates the probable phenomenon that might take place in presence of O2. In this research, we unveiled the outcomes of NRR in presence of O2. Furthermore, CO2 is the

fourth abundant gas in the atmosphere. Hence, we revealed the influence of this gas on NRR kinetics. Overall, this research discloses the catalysis, kinetics, and detecting efficiency of nitrate ions via a reduction reaction in the neutral medium in presence of O₂, CO₂ and N₂ gases utilizing a Cu modified gold electrode.

Experimental

Materials

All the chemicals used in this study were of analytical grade and were used as received without further purification. Sodium nitrate (NaNO₃) and copper sulphate pentahydrate (CuSO₄·5H₂O) were purchased from Merck, Germany, while the sulfuric acid (H₂SO₄) and alumina powder (Al₂O₃) were sourced from Sigma-Aldrich, Germany. For the preparation of sample solutions, we utilized Milli-Q pure water, ensuring low resistivity and high purity. The electrochemical investigations were conducted using the Autolab 128 N potentiostat (Netherlands) and CHI 660 potentiostats (USA). A silver chloride electrode saturated with KCl (Ag/AgCl sat. KCl) obtained from CHI instruments, USA was employed as the reference electrode. A platinum wire and a copper-modified gold electrode were respectively utilized as the counter electrode and the working electrode. A conventional 3-electrode system was assembled utilizing the above-mentioned reference, counter, and working electrodes to execute all the electrochemical experiments.

Characterization

Electrochemical characterization was performed by recording electrochemical impedance spectra (EIS) and open circuit potential (OCP). EIS measurements were taken over a frequency range of 0.1 Hz to 100 kHz with an excitation potential of -1.0 V vs. Ag/AgCl (sat. KCl). The electrode morphology was examined using a scanning electron microscope (SEM) (JSM-7610F, Japan). X-ray diffraction (XRD) patterns were obtained with a Rigaku SmartLab diffractometer utilizing Cu K α radiation ($\lambda = 1.5406$ Å). Energy dispersive X-ray (EDX) analysis was conducted with a TM3030Plus miniscope (Hitachi Ltd.). To determine the chemical states of Cu and Au on the

Cu/Au electrode, X-ray photoelectron spectra (XPS) were recorded using a delay-line detector (DLD) spectrometer (Kratos Axis Ultra; Kratos Analytical Ltd.) with an Al Kα radiation source (1486.6 eV). The XPS instrument was calibrated to 284.5 eV (C 1s).

Electrochemical experiments

At first, a gold electrode was polished on a polishing pad employing alumina powder (average particle diameter 0.3 µm) by rotating it clockwise and anti-clockwise, similar to the shape of the number eight('8'). The electrode had an exposed geometric surface area of 0.0314 cm². After polishing, the electrode was subjected to sonication for 20 minutes in 0.1 M H₂SO₄ solution at room temperature. Followed by the mechanical cleaning, the electrode surface went through electrochemical treatment which involved cycling the electrode in the potential range -1.4 to +1.2V vs. Ag/AgCl (sat. KCl) in 0.1 M NaOH solution for 30 times employing cyclic voltammetry (CV) method, followed by a second cycling in the range -0.2 to +1.5 V in 0.1 M H₂SO₄ solution for another 30 repetitive CV cycles. The scan rate applied for the scanning process was fixed at 0.1 Vs⁻¹. The process was repeated until overlapping characteristic cyclic voltammograms (CVs) for polycrystalline gold (Au) electrode was observed. The process of depositing copper (Cu) onto a mechanically and electrochemically cleaned Au surface involved cycling an Au electrode electrochemically in a 0.1 M CuSO₄ solution four times within the potential range 0 to -1.0 V at a scan rate of 0.1 Vs⁻¹. The CV potential cycling led to the accumulation of Cu particles on the Au surface. An illustration of the preparation steps of the proposed electrode is provided as **Scheme** S1 in ESI. The as-fabricated electrode will be denoted as Cu/Au electrode and will be utilized as the working electrode for further experiments in a 10 mL solution of 0.1 M KCl in an electrochemical cell. The influence of various gases, including O₂, N₂, and CO₂, was assessed by dissolving them through purging into a 10 mL KCl solution for 10 minutes at a flow rate of 50 mL/min from a central gas storage system. The quantitative measurement of ammonia-nitrogen was obtained employing a Milwaukee MI405 Ammonia Medium Range PRO Photometer (USA) instrument.

Results and discussion

Surface characterization

Surface morphology of the as-prepared Cu/Au electrode was unraveled using scanning electron microscope (SEM), energy-dispersive X-ray (EDX) analysis, and X-ray diffraction (XRD) analysis. The SEM images of the Cu/Au surface at two different magnifications are presented in **Figure 1(A-B)**. The images show that the size of the deposited Cu particles is in micrometer range, hence they can be addressed as Cu microparticles. The Cu microparticles are nearly evenly dispersed on the Au substrate taking a spherical shape. No agglomeration of particles on the surface is observed. The EDX elemental spectrum in **Figure 1C** discloses the elemental identification and atomic percentage of the Cu particles on Au surface. The ratio of atomic percent for Cu and O is 2.5:1, which indicates the existence of Cu₂O on the Au surface.

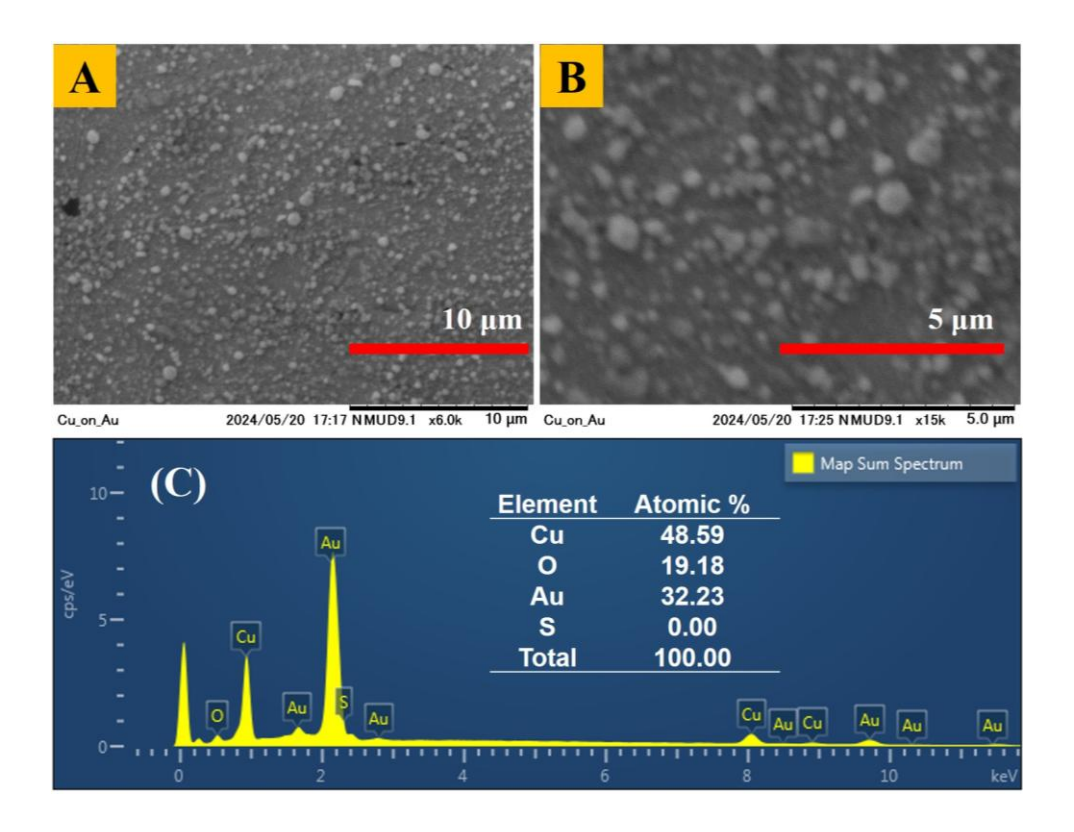


Figure 1. SEM images of the Cu/Au surface at (A) 6,000 and (B) 15,000 times magnification. (C) EDX elemental spectrum of the Cu/Au surface.

The X-ray photoelectron spectra (XPS) was analyzed to understand the chemical states of Cu and Au species on Cu/Au surface. **Figure 2A** demonstrates the fine scan XPS spectrum of Au substrate,

where peaks at 84.3 and 88.1 eV are identified as Au 4f_{7/2} and Au 4f_{5/2}, respectively, indicating zero valent metallic state of Au particles.^[56] The Cu 2p spectra in **Figure 2B** are composed of two well-resolved peaks located at 932.18 eV and 952.01 eV, corresponding to Cu 2p_{3/2} and Cu 2p_{1/2}, respectively. The peak positions closely match with those of Cu⁰ and Cu¹ species. The peaks appearing at binding energies of 934.31 and 954.09 eV are due to the existence of Cu^{II} species.^[57,58]

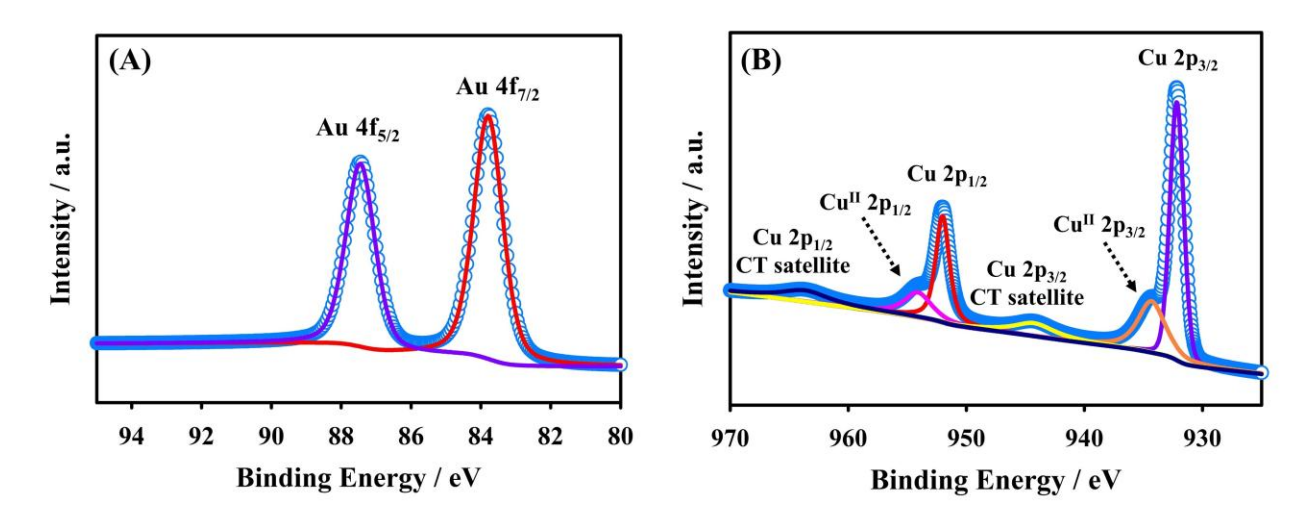


Figure 2. Deconvoluted XPS fine scan spectrum of (A) Au 4f orbital (B) Cu 2p orbital recorded for Cu/Au electrode surface.

The XRD is a reliable characterization technique to confirm the formation of crystalline structure. The XRD patterns shown in **Figure 3** reveal the crystalline facets of Cu and Au, which precisely match those of their respective metallic species.^[59,60] No secondary phases or impurities were detected in the XRD patterns. The comprehensive characterization analysis confirms that the gold substrate of the prepared electrode is completely polycrystalline and exists solely in its metallic form. In contrast, the deposited Cu microparticles are present in various oxidation states. The variation in oxidation states derived from different characterization techniques can be attributed to their differences in sensitivity.

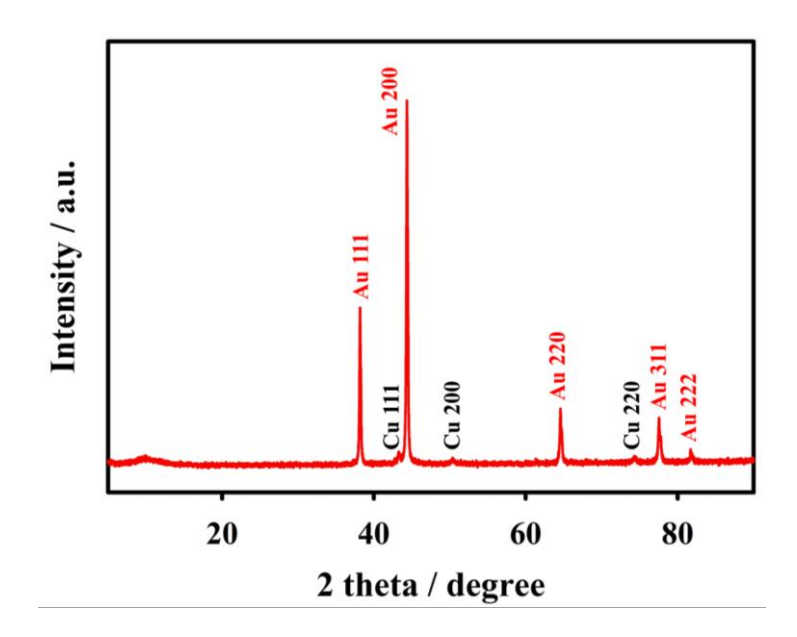


Figure 3. X-ray diffraction (XRD) patterns for the as-prepared Cu/Au electrode.

Open circuit potential

Measuring the open circuit potential (OCP) is essential for optimizing a reaction condition in a competition to deliver the most favorable experimental conditions. In an electrochemical system, OCP defines a potential at which no visible faradaic current flows across the electrode. Hence, it is the potential where both anodic and cathodic processes meet at the same rate.

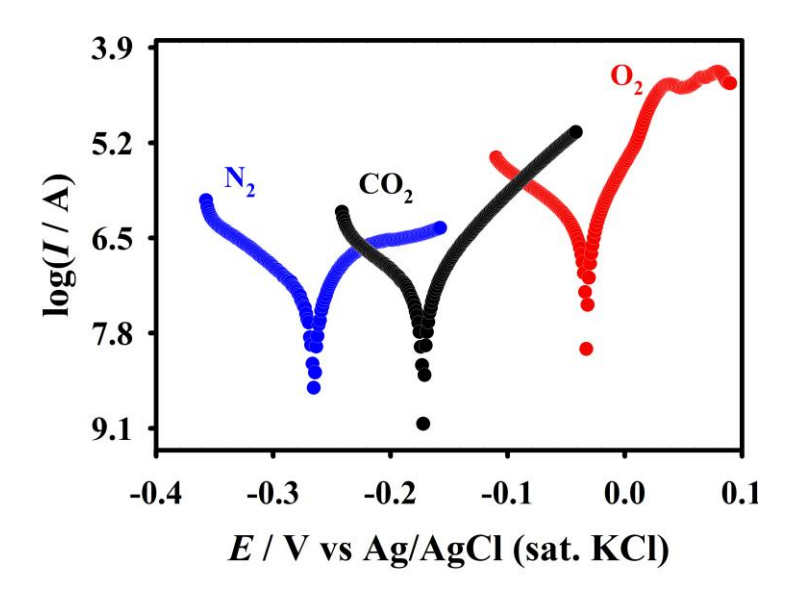


Figure 4. Normalized polarization curves of 3.0 mM NaNO₃ + 0.1 M KCl solution under O₂, N₂, and CO₂ saturated conditions recorded at a scan rate of 0.01 Vs⁻¹.

Figure 4 shows the normalized log(*I*) vs. *E* plots of 3.0 mM NaNO₃ + 0.1 M KCl solutions obtained by the Cu/Au electrode under N₂, O₂, and CO₂ saturated conditions separately. It can be observed from the figure that under O₂-saturated conditions, an OCP of −0.03 V was obtained for the electrode. When the same solution was saturated with CO₂ and N₂ gases separately, the OCP values shifted negatively to −0.17 and −0.27 V vs. Ag/AgCl (sat. KCl), respectively. This observation suggests that the existence of CO₂ gas can generate a reduction potential stronger than dissolved O₂ but weaker than the presence of N₂. However, it is also notable that the corrosion current exhibited by the Cu/Au electrode is maximum in the presence of dissolved O₂, where the dissolved CO₂ gas corrodes the electrode at the same rate as observed in the presence of dissolved N₂. This observation suggests that the stability of the Cu/Au electrode in the presence of N₂ or CO₂ might be better compared to its stability in the presence of O₂ under the given experimental conditions.

EIS studies

Electrochemical impedance spectroscopy (EIS) is crucial for investigating characteristics of an electrode with modified surface. The EIS spectra are analyzed to obtain the electrical properties of the electroactive species. This type of moiety undergoes an electron transfer phenomenon on the

surface of the working electrode. The total impedance was measured by three parameters: (1) electrolyte resistance (R_s), (2) double layer capacitance (C_{dl}), and (3) charge transfer resistance (R_{ct}). The complex impedance is commonly expressed as a sum of two components: the real part (Z_{re}) and the imaginary part (Z_{im}). These components are typically attributed to the resistance and capacitance of the cell, respectively. The components of the circuit, C_{dl} and R_{ct} , depend on the dielectric constant and insulating characteristics at the interface between the electrode and solution. In EIS, the semicircle's diameter corresponds to the electron transfer resistance value, denoted as R_{ct} . The resistance handles the kinetics at which electrons are moved between the redox probe and the electrode at their surface. The absorption of different substances on the electrode surface influences their kinetic values. The electrochemical study has been conducted by building a conventional three-electrode system to analyze the comparative binding properties of the Cu/Au catalyst in the presence of a supporting electrolyte.

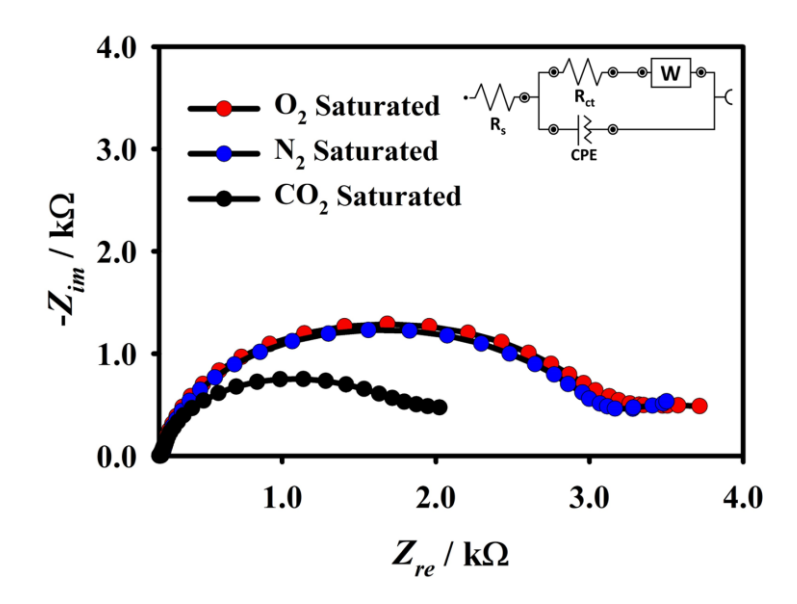


Figure 5. Nyquist plots of the Cu/Au electrode in 3.0 mM NaNO₃ + 0.1 M KCl solution under O₂, N₂, and CO₂ saturated conditions at an excitation potential of -1.0 V. The dotted lines represent experimental data and the solid lines represent fitted data (inset: relevant equivalent circuits).

The Nyquist plots in **Figure 5** displays the results acquired for the Cu/Au electrode in a 0.1 M KCl for a 3.0 mM $NO_3^- + 0.1$ M KCl solution at a potential of -1.0 V after saturating with O_2 , N_2 , and CO_2 . The R_s value of the solution under the experimental conditions did not significantly vary,

irrespective of the soluble gases present. However, measurable R_{ct} variation was observed. In the presence of dissolved CO_2 , the least charge transfer was observed, which is ca. 1.83 k Ω , followed by 2.82 k Ω and 2.93 k Ω in the presence of saturated N_2 and O_2 gases, respectively. The R_{ct} value exhibited by the carbonated nitrate solution suggests that the solubility of CO_2 gas can enhance the electrode-to-solution charge transfer, which might indicate the conception of a facile nitrate reduction reaction (NRR) rate compared to the O_2 or N_2 soluble condition.

NRR on Cu/Au electrode

The immobilization of Cu particles on the Au surface creates noble catalytic sites to execute NRR in the neutral medium (see ESI file, **Figure S1**). Hence, the fabricated Cu/Au electrode was employed to examine the influence of different dissolved gases on NRR. **Figure 6** shows the cyclic voltammograms (CVs) of 3.0 mM NaNO₃ in 0.1 M KCl solution, recorded at a scan rate of 0.1 Vs⁻¹ after saturating the solution with O₂, N₂, and CO₂ gases independently. Irrespective of the gas purged, the NRR took place in all conditions, displaying two consecutive waves denoted as E_{p1} and E_{p2} , respectively. The former wave defines the conversion of NO_3^- into NO_2^- (shown in **equation 1**) as this wave did not appear while NaNO₂ alone was used as a reactant (see **Figure S1**).

$$NO_{3-ad} + H_{2}O_{ad} + 2e^{-} \rightarrow NO_{2-ad} + 2OH_{ad}$$
 (1)

Furthermore, 50 mL 0.1 M NaNO₃ and 0.1 M NaNO₂ solutions prepared in 0.1 M KCl were bulk electrolyzed, applying a working potential of -1.2 V vs. Ag/AgCl (sat. KCl) to unveil the reason for the latter wave's appearance. After two hours of electrolysis, the appearance of ammonia was observed as an end product by spectroscopic method irrespective of whether nitrate or nitrite was used as a reactant. A detailed measurement procedure of NH₃-N is provided in **Text S1**. For further confirmation, the XPS fine scan spectrum for N 1s region was obtained that revealed adsorbed NH₃ on the Cu/Au electrode surface as shown in **Figure S5**. Note that the probable reaction products for NO₃⁻ reduction reaction are NO₂⁻, NO, NOH, HNOH, NH₂OH, and NH₃. [62,63] The oxidation states of nitrogen for reaction products NO₂⁻, NO, NOH, HNOH, and NH₂OH range from +3 to -1, while NH₃ has the most negative oxidation state of -3. A previous study found that

NO₃ with an oxidation state of +5 gives a peak with binding energy of 407.3 eV in the N 1s region of XPS spectrum. [64] The study further revealed that a peak with lower binding energy of 405.9 eV can be assigned to +4 oxidation state of nitrogen. A binding energy between 400 and 402 eV indicates reduced nitrogen species in the range of nitrogen oxidations states spanning +1 to -1. However, in our case, we obtained two deconvoluted N 1s peaks even at lower binding energy values, 398.19 and 399.71 eV, indicating nitrogen species having a more negative oxidation state than -1. The only species possible with a more negative oxidation state than -1 is NH₃, which has a nitrogen with oxidation state of -3. Therefore, NH₃ is likely the predominant species adsorbed on the Cu/Au surface after electrocatalytic NRR. Similar two characteristic peaks for adsorbed NH₃ species at binding energies of about 398.19 and 399.71 eV were also observed in previous studies. [65,66] These observations suggest that at E_{p2} wave, the reactions shown by **equation 2** and **3** occurred.

$$NO_{2-ad}^{-} + 5H_{2}O_{ad}^{-} + 6e^{-} \rightarrow NH_{3-ad}^{-} + 7OH_{ad}^{-}$$
 (2)

$$NO_{3-ad}^{-} + 6H_{2}O_{ad}^{-} + 8e^{-} \rightarrow NH_{3-ad}^{+} + 9OH_{ad}^{-}$$
 (3)

The positions of the peaks and corresponding currents under different gas saturation conditions are tabulated in **Table 1**.

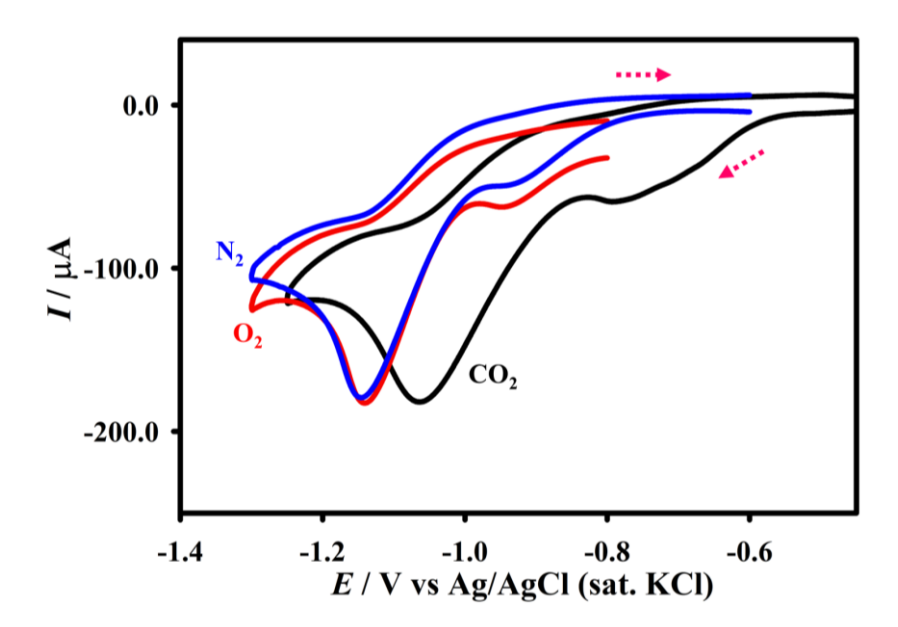


Figure 6. Cyclic voltammograms (CVs) of 3.0 mM NaNO₃ in 0.1 M KCl recorded with a Cu/Au electrode at a scan rate of 0.1 Vs^{-1} in various gas saturated solutions.

Table 1 Kinetic properties of NRR obtained with Cu/Au electrodes in the presence of different dissolved gases.

Dissolved gas	Tafel slope	E _{p1} properties			E _{p2} properties		
	b/ mV dec ⁻¹	-E _{p1} /V	$-I_{pl}/\mu A$	$\Delta G_p^{\ddagger}/\mathrm{eV}$	-E _{p2} /V	$-I_{p2}/\mu A$	$\Delta G_p^{\ddagger}/\mathrm{eV}$
O_2	415	0.94	42.18	0.337	1.14	167.7	0.339
$\overline{ m N_2}$	168	0.94	42.83	0.337	1.14	172.7	0.340
CO_2	141	0.71	38.29	0.336	1.06	170.7	0.343

Figure S2 presents CVs recorded in presence and absence of NO_3^- ions in various gas saturated 0.1 M KCl solutions. In the presence of dissolved gases, the area under E_{p1} increased with an order of $O_2 \le N_2 \le CO_2$. Besides, the position of the E_{p1} peak appeared at a relatively positive potential of -0.71 V under CO₂ conditions, while this peak was found to appear at -0.94 V both in the presence of O₂ and N₂ gases. It is worth noting that CO₂ reduction reaction takes place at -0.76 V on Cu/Au surface as shown in **Figure S3**, which is very close to the reduction potential of NO_3^- . Thus, one might expect interference from CO₂ reduction reaction during NRR in CO₂ saturated solution. However, interestingly, the E_{p2} peak current arising from NO_2^- to NH_3 reduction in case of CO₂ saturated condition (170.7 μ A), which comes after E_{p1} peak for NO_3^- to NO_2^- reduction, is almost similar to that of E_{p2} peak current in N_2 saturated solution (172.7 μ A), as shown in Figure 6 and Table 1. This observation indicates that although NRR can potentially experience some hindrance from CO₂ reduction reaction, as demonstrated by the broadening of the E_{p1} peak in CO₂ saturated solution compared to E_{p1} in N₂ saturated solution, the interference is somehow compensated by other ways. As a result, sufficient NO_2^- is produced at E_{p1} to undergo further reduction at E_{p2} to generate comparable current with that of hindrance-free N₂ saturated solution. Moreover, in presence of CO₂, the NRR process became kinetically facile requiring the least overpotential. Although broadening of E_{p1} peak is also observed in case of O₂ saturated solution indicating some interference from O₂ reduction reaction (see Figure S2), but in this case, the peak potential for both NO_3^- and NO_2^- reduction remained the same with that of N_2 condition. Moreover, O_2 saturated solution exhibited the least current for both E_{p1} (42.18 μ A) and E_{p2} (167.7 μ A). Thus, no kinetic advantage is anticipated in presence of O_2 during NRR. In presence of N_2 gas, NRR showed the maximum current (172.7 μ A) at -1.14 V as no such interference occurs from N_2 (check **Figure S3**). Note that a bare Au electrode does not show any NRR activity, whereas NRR follows a very complex route on a bare Cu electrode, converting nitrate directly to ammonia, making it difficult for kinetic investigation. In comparison, the kinetic study is more facile on a Cu/Au electrode where much lesser complex process take place. Comparative CVs for these electrodes are shown in **Figure S4**.

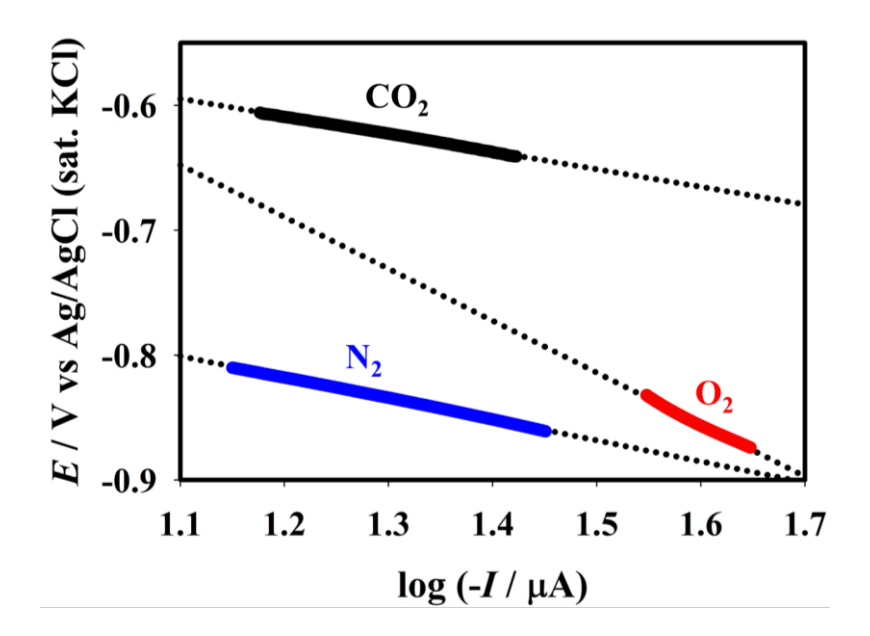


Figure 7. Tafel plots of NRR process over Cu/Au electrode in the presence of different dissolved gases. The data for plotting these curves were extracted from **Figure 6**.

In order to evaluate electron transfer kinetics, Tafel slope was calculated as per equation 4.

$$\log(I) = \log(I_0) - \frac{\alpha F}{2.303 RT} (E - E^{\circ})$$
(4)

where, $E^{\circ\prime}$ is formal potential, E is the applied potential (vs Ag/AgCl), $b = \frac{-2.303RT}{\alpha F}$ is the Tafel slope, and $I_o = nFACk^{\circ}$ is the exchange current while $E = E^{\circ\prime}$. By studying the Tafel plots in **Figure 6**, the value of E was found to be 415, 168, and 141 mV dec⁻¹ in the presence of O₂, N₂,

and CO₂ gases, respectively. This statement signifies that O₂ adsorption impedes the rate of electron transfer. Furthermore, a chemical step follows during the rate-determining step. Since O₂ molecules readily adsorb onto the Cu/Au electrode surface, effectively blocking NO₃⁻ ions from accessing the electrode surface. This adsorption prevents the NO₃⁻ ion concentration at the electrode surface from reaching equilibrium with the bulk solution and consequently, a higher potential is required. Meanwhile, electron transfer becomes faster in the presence of N₂ as well as CO₂ gases and the least overpotential is required to amplify the reduction current by ten times. In the presence of N₂ and CO₂ gases, a single electron transfer involved at the rate-determining step as *b* is very close to 120 mVdec⁻¹.

Finally, activation free energy (ΔG_p^{\dagger}) at peak (E_p) was evaluated according to **equation 5**.

$$\Delta G_p^{\ddagger} = \frac{RT}{F} \left[\ln \left(Z_f \sqrt{\frac{RT}{F\alpha\nu D}} \right) - 0.78 \right] \tag{5}$$

where, $Z_f = \sqrt{RT/2\pi M}$ (M is the molar mass of nitrite), α is the transfer coefficient (estimated from peak width, i.e., $\alpha = 1.8 \text{RT}/F(E_{p1} - E_{p1/2})$, and other symbols have their usual meanings. **Table 1** displays that the value of ΔG_p^{\ddagger} relevant to NRR decreased with the introduction of different gases, with O₂ and N₂ having an identical outcome and CO₂ having a comparatively lower outcome (O₂ ~ N₂> CO₂). Meanwhile, the order of ΔG_p^{\ddagger} at E_{p2} exhibited an order of O₂ <N₂< CO₂.

From the above discussion, it can be inferred that dissolved gases influence the NRR process differently. The adsorption of O_2 gas made the Cu/Au electrode least active pertaining to the conversion of NO_3^- into NO_2^- exhibiting a large Tafel slope and the highest activation energy. On the other hand, NRR at E_{p1} proceeded with the least Tafel slope and activation free energy change magnitude in CO_2 saturated environment. Such event can be accounted to the acidic nature of CO_2 , which can neutralize the OH^- ions generated due to the reactions shown by **equation 1** and **2**, resulting in the formation of carbonate as per **equation 6**.

$$20H^{-} + CO_{2} \to CO_{3}^{2-} + H_{2}O \tag{6}$$

In our previous study, we have shown that NRR causes an elevation in the pH of the medium from 7.0 to 12.5. [46] However, pH of the medium remained almost constant around 6 in the present case, supporting the scavenging of OH⁻ by the CO₂ molecules. The neutralization of ions by CO₂ molecules from the electrode-electrolyte interface makes the NRR process more favorable on Cu/Au surface and shifts executing potentials of reactions (E_{p1} and E_{p2}) shown by **equation 1** and **2** to relatively positive values compared to those exhibited in presence of N₂ or O₂ gases. The neutralization of OH^- allowed **equation 1** to proceed at the lowest potential of -0.73 V with the least Tafel slope and ΔG_p^{\ddagger} values. However, shortly after passing E_{p1} , the potential scanning reached the reduction potential of CO₂ molecules at -0.76 V (see **Figure S2** and **Figure S3**). This event presumably made the **equation 2** for nitrite to ammonia reduction that would take place at -1.06 V, competitive with the preceding CO₂ reduction on the Cu/Au surface. Hence, compared to N₂ or O₂ gas saturated condition, a relatively higher ΔG_p^{\ddagger} was observed for NRR at E_{p2} in CO₂ saturated condition.

Contrarily, N_2 gas displayed strong chemical and electrochemical inertness under experimental conditions and did not adhere to the Cu/Au surface. The purging of N_2 gas effectively dispelled dissolved O_2 gas molecules from the solution. This action prevented the deactivation of the electrode surface under N_2 environment, thereby enhancing the electron transfer kinetics of the reaction (2) and exhibiting the least ΔG_p^{\ddagger} at E_{p2} in reference to the CO_2 saturation condition. However, since we observed the least corrosion current, least charge transfer resistance (R_{ct}), least Tafel slope magnitude, least activation free energy (ΔG_p^{\ddagger}), and least over potential for CO_2 saturated situation, hence, further kinetic investigation was conducted under CO_2 saturated condition.

NRR mechanism

The previous section revealed that the NRR process yielded ammonia as the end product via two consecutive reactions shown by **equation 1** and **2**, which are two and six-electron processes, respectively. The mechanism of the six-electron transfer process is highly complex, which is

beyond the scope of this study. Hence, in this section, the mechanism of **equation 1** has been sorted out under the CO_2 condition. For this purpose, scan rate variant CVs were recorded for 3.0 mM NaNO₃ in 0.1 M KCl shown in **Figure 8A**. **Figure 8B** demonstrates that the current increment at both peaks (E_{p1} and E_{p2}) is proportional to the square root of the scan rate. This means that the NRR at both peaks was limited by mass transfer.

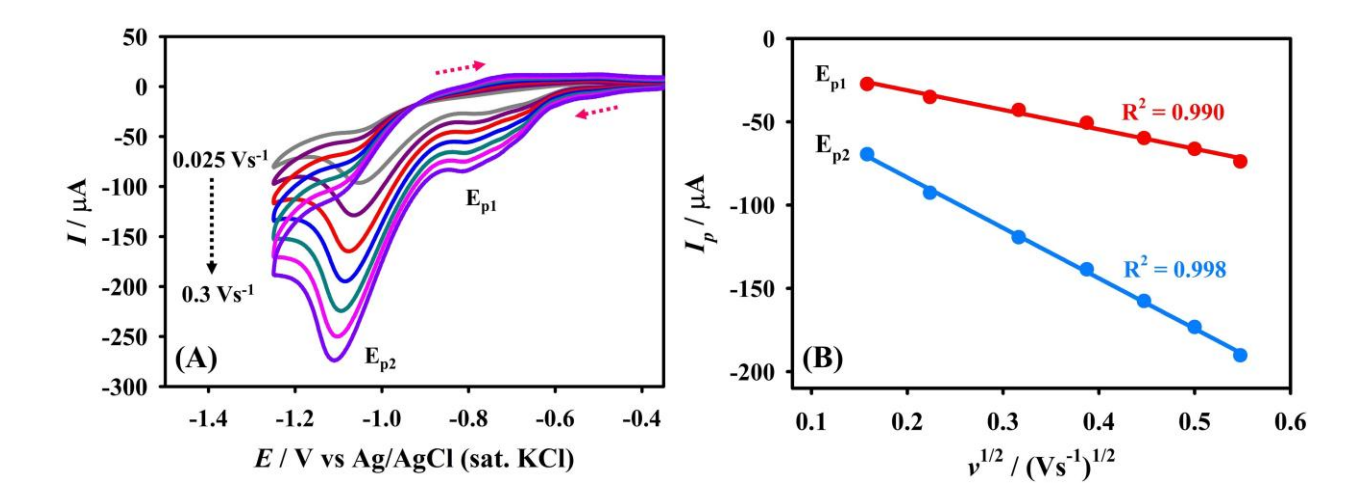


Figure 8. (A) CVs of 3.0 mM sodium nitrate in 0.1M KCl at variable scan rates (0.025 to 0.3 Vs⁻¹). (B) Dependency of peak current (I_p) on square root of scan rate (ν).

Subsequently, $I_{pl}/v^{1/2}$ vs. v plot is illustrated in **Figure 9**, where I_{pl} is the peak currents at E_{pl} at variable scan rates and v is the scan rate.

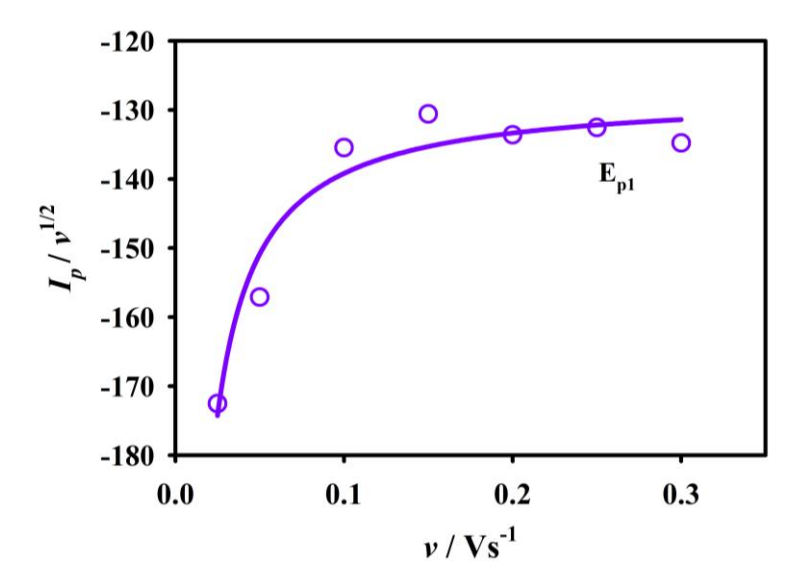


Figure 9. Plot of $I_p/v^{1/2}$ against v at E_{p1} for CO_2 saturated condition. Data were extracted from Figure 8A.

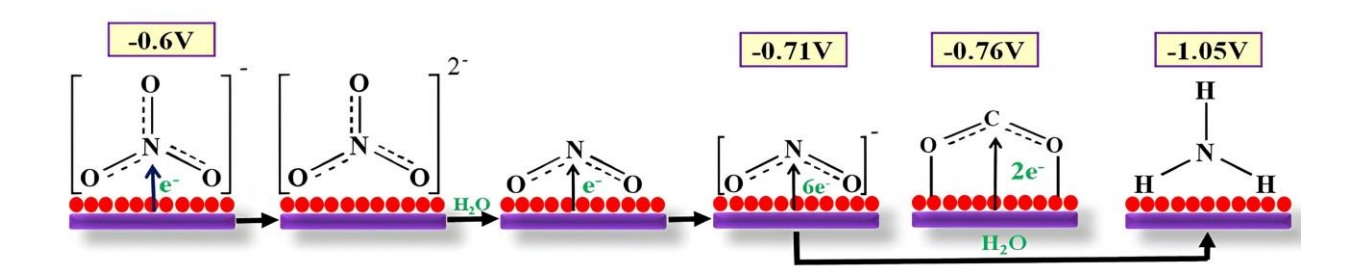
Ideally, $I_p/v^{1/2}$ against v should remain constant for a mass transfer limited process. However, **Figure 9** shows that as the scan rate increases, the value of $I_p/v^{1/2}$ decreases. Such observation indicates the presence of a catalytic mechanism during the NRR process, where a pre-equilibrium occurs between NO_3^- ions and a potential intermediate (possibly NO_3^{2-}). At slower scan rates (lower than 0.1 Vs^{-1}), the intermediate population becomes higher and the current becomes larger than the Randles Sevick equation predicted. [67,68] Meanwhile, at faster scan rates, due to time constraints, the population of the intermediate cannot become sufficient, as indicated by the Randles Sevick equation. Consequently, the value of the $I_p/v^{1/2}$ ratio reached a minimum at $v > 0.1 \text{ Vs}^{-1}$. Furthermore, the transfer coefficient (α) from the peak separation was calculated to be 0.57 w.r.t. E_{p1} . As the value of α is higher than 0.5, it implies that a consecutive process was involved around the peak potential (E_{p1}). [69] Since the conversion of NO_3^- into NO_2^- involves a two-electron transfer process, the following stepwise mechanism shown by **equation 7(i)-7(iii)** could be inferred.

$$NO_3^- + e^- \rightleftharpoons NO_3^{2-}$$
 (rds) 7(i)

$$NO_3^{2-} + H_2O \rightarrow NO_2 + 2OH^-$$
 7(ii)

$$NO_2 + e^- \rightarrow NO_2^-$$
 7(iii)

The NO_2^- ions formed following the above mechanism at E_{p1} later reduced to NH_3 by receiving six electrons at E_{p2} . Based on the above discussion, most feasible route showing the influence of dissolved CO_2 gas on NRR process is shown by a diagram in **Scheme 1**.



Scheme 1. Schematic diagram showing the NRR reaction route on Cu/Au surface in presence of dissolved CO₂ gas during potential scanning.

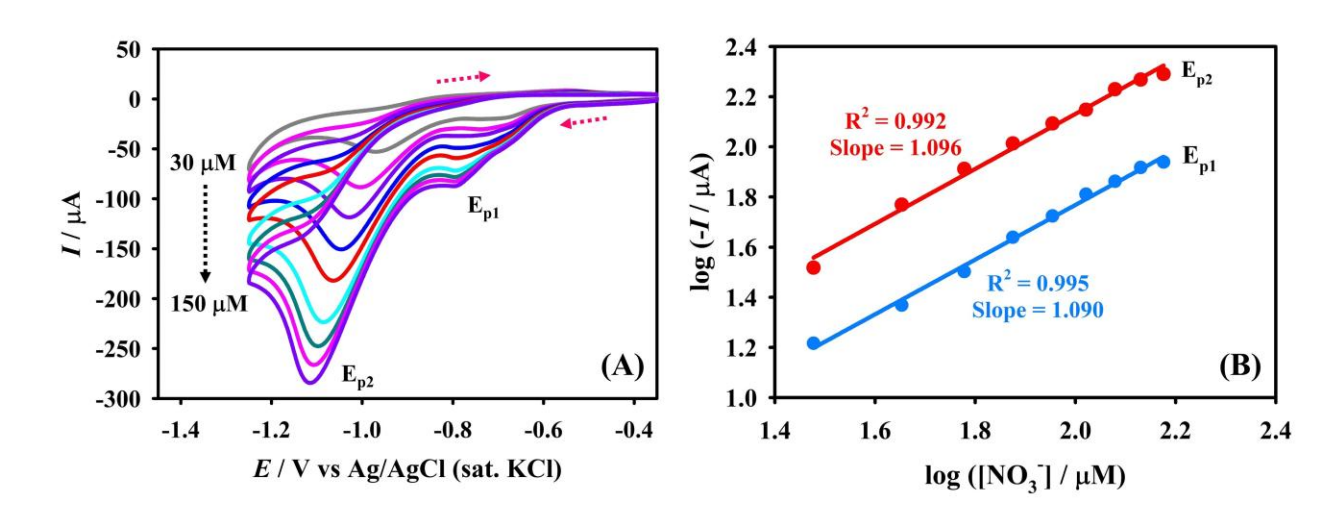


Figure 10. (A) CVs obtained varying the concentration of NaNO₃ using the Cu/Au electrode at a scan rate of 0.1 Vs⁻¹. (B) Plot showing dependency of log (-I) on log [NO_3^-] at peak E_{p1} and E_{p2}.

The kinetic order of reaction, expressed by the symbol m, is a crucial parameter to understand the mechanistic pathway of an electrochemical system. The kinetic order can be accurately calculated by investigating the correlation between the concentration of the electro-active moiety and peak current studies. A linear pattern should be observed in the $\log(I)$ vs. $\log[NO_3^-]$ curve in accordance with **equation 8** shown below. This equation is valid in electrochemistry analysis to comprehend the dynamics and mechanisms of electrochemical systems.

$$\log(I) = \log(k) + m\log[NO_3^-] \tag{8}$$

Here, the reaction rate constant is denoted by 'k' and the order of reaction as 'm'. The slope of the log(-I) vs. $log[NO_3^-]$ linear plot as demonstrated in **Figure 10B** gave us the reaction order for both process occurring at E_{p1} and E_{p2} , which were found to be 1.090 and 1.096, respectively (with $R^2 = 0.99$), which are fairly close to 1. Thus, it can be concluded that both processes at E_{p1} and E_{p2} take place following a first-order reaction kinetics on Cu/Au surface.

Detection of nitrate

Sensing performance

The limit of detection (LOD) and linearity can be explored from the graphs of concentration-dependent differential pulse voltammogram (DPVs) as shown in **Figure 11A**. The elevation in peak current (I_p) under experimental condition exhibited a linear relation with the NO_3^- concentration as depicted in **Figure 11B**. This relationship was observed within the concentration range of 0 to 90 μ M NaNO₃. LOD for nitrate detection was determined using **equation 9** which was found to be 0.46 μ M with a signal-to-noise ratio (S/N) of 3. The sensitivity value of the electrode for NO_3^- detection was measured to be 3.49 \times 10⁻¹ μ A μ M⁻¹.

$$LOD = \frac{3 \times SD}{SR}$$
 (9)

Where SD refers to standard deviation of current values found for three blank measurements and SR stands for slope of the regression line shown in **Figure 11B**.

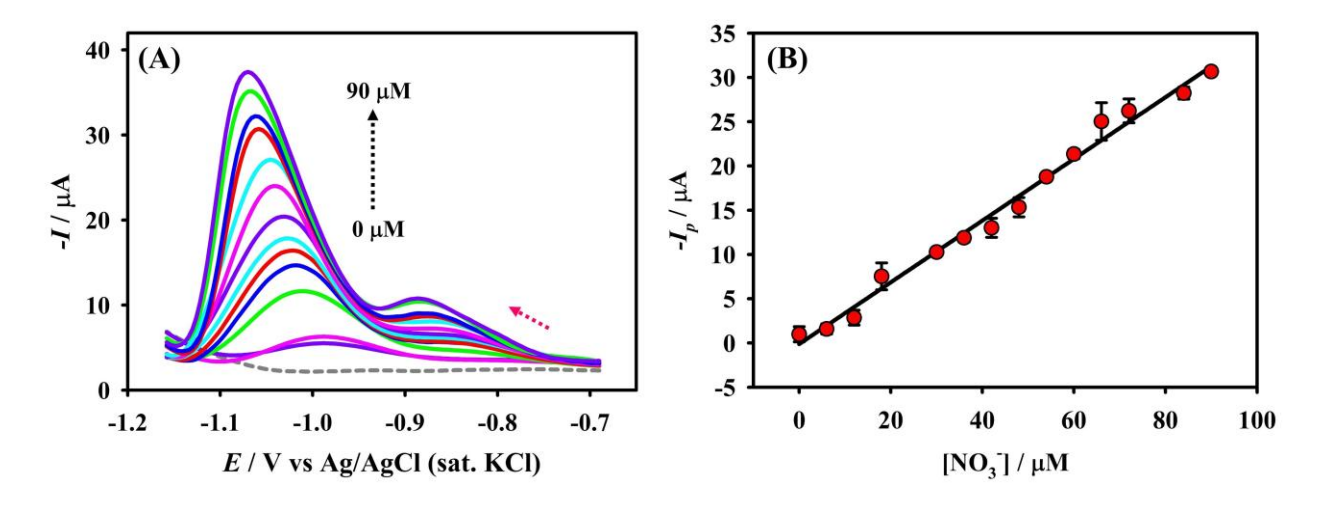


Figure 11. (A) Differential pulse voltammograms (DPVs) for NRR at variable NaNO₃ concentrations (0-90 μM) recorded using Cu/Au electrode in CO₂ saturated 0.1 M KCl solution fixing a scan rate of 0.1 Vs⁻¹. (B) Variation of peak current (I_p) with varying NO_3^- concentration derived from DPVs.

The performance of the Cu/Au electrode as nitrate sensor is comparable with that of various previously documented nitrate sensing electrodes as demonstrated in **Table 2**. The table data clearly demonstrates that under the proposed experimental condition, the as-prepared electrode achieved one of the lowest LODs documented for nitrate detection.

Table 2 The comparative scenario of nitrate sensors utilizing different electrodes.

Electrode	Technique	LDR (µM)	LOD (µM)	pН	Ref.
Cu nanoparticles electrodeposited on polypyrrole-polystyrene sulfonate polyethyleneimine-functionalized multiwall carbon nanotubes	CA ^[a]	100-5000	30	7	[70]
Ag dooped zeolite expanded graphite-epoxy	CV	1000-10000	100	7	[71]
Porous Cu-Ni alloy and Rh modified Cu porous layer	CA	20-1000	-	7 and 13	[72]
Ag nanoparticles electrodeposited on Au electrode	SWV ^[b]	0.39-50	0.39	7	[73]
Ag nanoparticles electrodeposited on Au electrode	SWV	0.9×10 ⁻³ -	0.9×10 ⁻³	6	[74]

Cu nanostructure on pencil graphite electrode	CA	1-35	0.59	2	[75]
Cu deposited on carbon fibre	SWV	3-2000	1.1	2	[76]
Copper-electrodeposited gold electrode	DPV	20–800	0.52	<1.0	[53]
Copper-electrodeposited on gold	DPV	0-90	0.46	7	This
electrode					work

[[]a] Chronoamperometry; [b] Square wave voltammetry.

Nitrate detection in real samples

Method validation of the detector in daily-life specimen study was performed using the asfabricated Cu/Au electrode through the standard addition method. As a representative of a wide range of available water sources, irrigation water, laboratory tap water and canal water specimens were investigated for NRR study. **Table 3** displays the outcomes acquired from the study by repeating each sample thrice under similar experimental condition. Excellent recovery of nitrate (99.09 - 102.30%) demonstrates the efficiency and reliability of the proposed Cu/Au electrode for nitrate detection.

Table 3 Quantifying nitrate ions in daily-life specimens utilizing Cu/Au electrode.

Specimen	Added (µM)	Acquired ^[a] (μM)	RSD ^[b] (%)	Recovery ^[c] (%)
Irrigation water	49.95	50.70	3.05	101.5
Tap water	49.95	49.50	2.84	99.09
Canal water	49.95	51.10	3.40	102.30

[[]a] Mean of repeated result (S/N = 3); [b] Relative standard deviation (RSD) indicates the precision of acquired data; [c] Recovery = ($[NO_3^-]$ determined/ $[NO_3^-]$ taken) × 100%.

Stability study

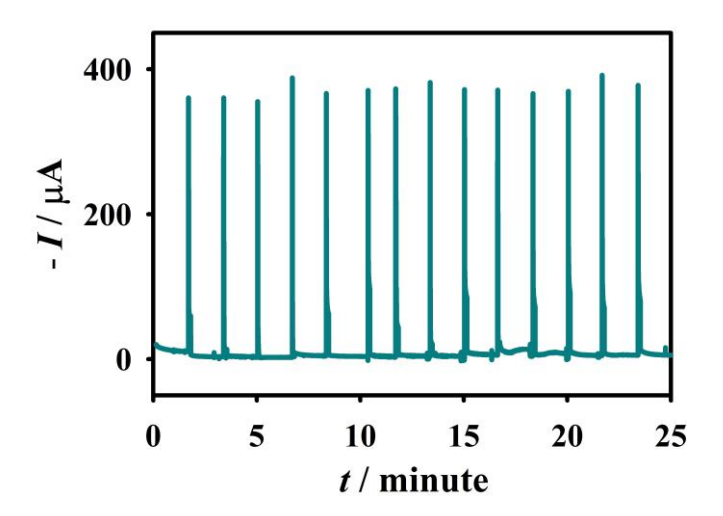


Figure 12. Chronoamperograms documented by repeatedly injecting 100 μL of 0.1 M NaNO₃ onto the Cu/Au electrode surface at a fixed time interval.

The stability of electrodes plays an integral role in the electrochemical process. It is a critical factor that defines the overall performance and dependability of the system and thus requires careful consideration. Hence, batch injection analysis (BIA) was performed for the stability study. BIA involved injecting CO₂ saturated 100 μL of 0.1 M NaNO₃ onto the surface of the electrode, which in turn created a temporary electrolysis zone. The BIA analysis was conducted for a continuous 25 minutes at an applied potential of −1.06 V vs. Ag/AgCl (sat. KCl). The reproducibility of the resulting reduction current as demonstrated by the *i-t* curve in **Figure 12** confirms the stability of the electrode over an extended period. The recorded signal exhibits a peak-shaped response that fades quickly to baseline due to the diffusion out effect of reaction product from the electrode surface to the bulk of the electrode. The extent of these signals is proportional to nitrate concentration added. Such constancy of the current intensities over an extended period under the applied potential imply that the efficiency of the Cu/Au electrode retains even after multiple measurement. Thus, the proposed electrode can be employed for routine analysis to accurately detect nitrate in various samples.

Conclusion

In this study, we investigated the influence of dissolved N₂, O₂, and CO₂ gases in a neutral pH reaction medium during the nitrogen reduction reaction (NRR). Our findings revealed that N₂ does

not hinder the NRR, whereas O_2 slightly interferes with the reduction of nitrate to nitrite, subsequently decreasing the nitrite to ammonia reduction current. In contrast, CO_2 neutralizes OH^- ions, enabling both nitrate and nitrite reduction processes to occur at a lower potential compared to N_2 and O_2 saturated conditions. This phenomenon facilitates the conversion of NO_3^- to NO_2^- on a Cu/Au surface by lowering the Tafel slope magnitude and the free energy of activation. Further investigation under CO_2 saturated conditions revealed that both reduction waves followed first-order, diffusion-limited kinetics. Utilizing the electrode as a sensing device for NO_3^- in a neutral medium demonstrated an ultra-low limit of detection (LOD) of $0.46~\mu M$ and a sensitivity of $3.49 \times 10^{-1}~\mu A~\mu M^{-1}$ in the linear range of 0 to 90 μM . These findings suggest that the Cu/Au electrode is well-suited for routine nitrate analysis in neutral water sources, benefiting from the prevalent CO_2 environment to achieve precise and sensitive measurements.

Acknowledgement

The authors acknowledge the Researchers Supporting Project number (RSPD2024R674), King Saud University, Riyadh, Saudi Arabia for funding this research work. Ministry of Science and Technology (SGR-236674, Serial No 674, FY 2023-24), Bangladesh and Shahjalal University of Science Technology research center (Grant No. PS/2023/1/02) are also acknowledged for a partial support.

Author Contributions

Motasim B. Islam: Experimental, data analysis, writing – original draft, Mohammad Imran Hossain: Writing – original draft, data analysis, preparation of figures, Nazmul Hosen: Review and editing, Mostafizur Rahaman: Review and editing, funding acquisition, Nayan Ranjan Singha: Review and editing, Kentaro Aoki: Material characterization, Yuki Nagao: Material characterization, Mohammad A. Hasnat: Writing – original draft, conceptualization, review and editing, supervision, funding acquisition.

Conflict of Interests

The authors declare no conflict of interest.

Data Availability Statement

Data will be made available on request.

Keywords: Nitrate reduction reaction; Neutral medium; Dissolved gas; Nitrate sensor; Kinetics.

References

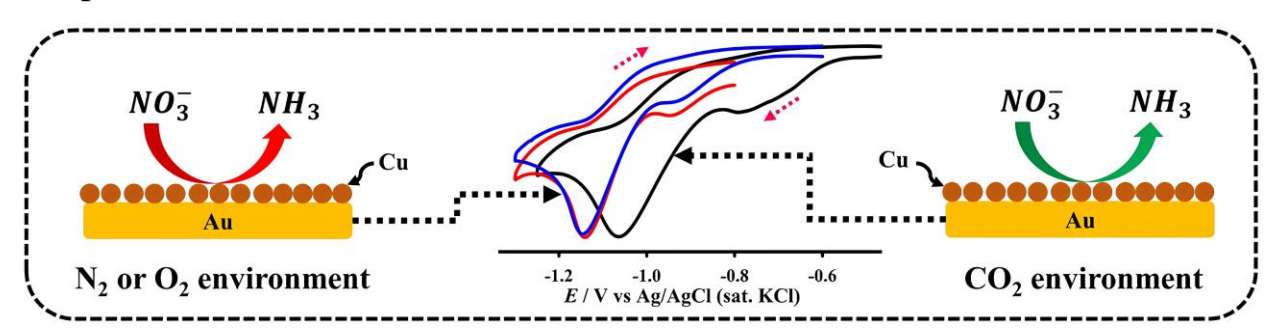
- [1] M. K. Samantara, R. K. Padhi, M. Sowmya, P. Kumaran, K. K. Satpathy, *Groundw. Sustain. Dev.* **2017**, *5*, 49–58.
- [2] P. Li, D. Karunanidhi, T. Subramani, K. Srinivasamoorthy, *Arch. Environ. Contam. Toxicol.* **2021**, *80*, 1–10.
- [3] M. I. Hossain, A. Bukhari, H. Almujibah, M. M. Alam, M. N. Islam, T. A. Chowdhury, S. Islam, M. Joardar, T. Roychowdhury, M. A. Hasnat, *J. Environ. Manage.* **2023**, *348*, 119381.
- [4] M. I. Hossain, M. A. Hasnat, *Heliyon* **2023**, *9*, e19299.
- [5] M. Luo, X. Liu, N. Legesse, Y. Liu, S. Wu, F. X. Han, Y. Ma, *Water, Air, Soil Pollut.* **2023**, *234*, 657.
- [6] M. Zhang, G. Huang, C. Liu, Y. Zhang, Z. Chen, J. Wang, J. Hydrol. 2020, 582, 124528.
- [7] H. G. Hoang, B. T. P. Thuy, C. Lin, D.-V. N. Vo, H. T. Tran, M. B. Bahari, C. T. Vu, *Chemosphere* **2022**, *300*, 134514.
- [8] B. F. Terjesen, in Fish Larval Physiol., CRC Press, 2020, pp. 263–302.
- [9] W. Zhao, X. Bi, M. Bai, Y. Wang, *Bioprocess Biosyst. Eng.* **2023**, 46, 621–633.
- [10] J. W. Drozd, *Divers. Bact. Respir. Syst.* **2018**, 87–112.
- [11] A. E. Laloo, J. Wei, D. Wang, S. Narayanasamy, I. Vanwonterghem, D. Waite, J. Steen, A. Kaysen, A. Heintz-Buschart, Q. Wang, *Environ. Sci. Technol.* **2018**, *52*, 5386–5397.
- [12] J. W. Erisman, J. N. Galloway, S. Seitzinger, A. Bleeker, N. B. Dise, A. M. R. Petrescu, A. M. Leach, W. de Vries, *Philos. Trans. R. Soc. B Biol. Sci.* **2013**, *368*, 20130116.
- [13] R. Pashaei, P. Zahedipour-Sheshglani, R. Dzingelevičienė, S. Abbasi, R. M. Rees, *Environ. Monit. Assess.* **2022**, *194*, 105.
- [14] J. N. Galloway, A. M. Leach, A. Bleeker, J. W. Erisman, *Philos. Trans. R. Soc. B Biol. Sci.* **2013**, *368*, 20130120.
- [15] A. Mosier, J. K. Syers, J. R. Freney, Agriculture and the Nitrogen Cycle: Assessing the Impacts of Fertilizer Use on Food Production and the Environment, Island Press, 2013.
- [16] M. Lu, Y. Yang, Y. Luo, C. Fang, X. Zhou, J. Chen, X. Yang, B. Li, *New Phytol.* **2011**, *189*, 1040–1050.
- [17] A. E. Ghaly, V. V Ramakrishnan, *J. Pollut. Eff. Control* **2015**, *3*, 1–26.
- [18] F. Bouraoui, B. Grizzetti, Sci. Total Environ. 2014, 468, 1267–1277.
- [19] S. E. Hobbie, J. C. Finlay, B. D. Janke, D. A. Nidzgorski, D. B. Millet, L. A. Baker, *Proc. Natl. Acad. Sci.* **2017**, *114*, 4177–4182.
- [20] C. Yu, X. Huang, H. Chen, H. C. J. Godfray, J. S. Wright, J. W. Hall, P. Gong, S. Ni, S.

- Qiao, G. Huang, Nature 2019, 567, 516-520.
- [21] M. M. Mekonnen, A. Y. Hoekstra, Environ. Sci. Technol. 2015, 49, 12860–12868.
- [22] A. Damar, A. Ervinia, F. Kurniawan, B. Y. Rudianto, in *IOP Conf. Ser. Earth Environ. Sci.*, IOP Publishing, **2021**, p. 12010.
- [23] V. C. Kapsalis, I. K. Kalavrouziotis, *Chem. Lake Restor. Technol. Innov. Econ. Perspect.* **2021**, 1–21.
- [24] World Health Organization, "Nitrate and nitrite in drinking-water: Background document for development of WHO Guidelines for Drinking-water Quality," 2003.
- [25] S. Fossen Johnson, in *Nitrate Handb.*, Taylor & Francis, **2022**.
- [26] R. McNulty, N. Kuchi, E. Xu, N. Gunja, J. Food Sci. 2022, 87, 1423–1448.
- [27] H. I. Shuval, N. Gruener, in *Proc. Conf. Nitrogen as a Water Pollut.*, Elsevier, **2013**, pp. 183–193.
- [28] J. A. Jones, A. O. Hopper, G. G. Power, A. B. Blood, *Pediatr. Res.* **2015**, *77*, 173–181.
- [29] O. Korostynska, A. Mason, A. Al-Shamma'a, Int. J. smart Sens. Intell. Syst. 2012, 5, 149–176.
- [30] T. P. Burt, N. J. K. Howden, F. Worrall, M. J. Whelan, *J. Environ. Monit.* **2010**, *12*, 71–79.
- [31] M. H. Ward, R. R. Jones, J. D. Brender, T. M. De Kok, P. J. Weyer, B. T. Nolan, C. M. Villanueva, S. G. Van Breda, *Int. J. Environ. Res. Public Health* **2018**, *15*, 1557.
- [32] M. E. E. Alahi, S. C. Mukhopadhyay, Sensors Actuators A Phys. 2018, 280, 210–221.
- [33] H. Small, *Ion Chromatography*, Springer Science & Business Media, **2013**.
- [34] M. R. Khan, S. M. Wabaidur, Z. A. Alothman, R. Busquets, M. Naushad, *Talanta* **2016**, 152, 513–520.
- [35] J. Choosang, A. Numnuam, P. Thavarungkul, P. Kanatharana, T. Radu, S. Ullah, A. Radu, Sensors 2018, 18, 3555.
- [36] M. F. Khanfar, W. Al-Fagheri, A. Al-Halhouli, Sensors **2017**, 17, 2345.
- [37] U. T. Yilmaz, G. Somer, *Gazi Univ. J. Sci.* **2016**, *29*, 285–291.
- [38] P. Singh, M. K. Singh, Y. R. Beg, G. R. Nishad, *Talanta* **2019**, *191*, 364–381.
- [39] H. Karimi-Maleh, F. Karimi, M. Alizadeh, A. L. Sanati, *Chem. Rec.* **2020**, *20*, 682–692.
- [40] Z. Wang, D. Richards, N. Singh, Catal. Sci. Technol. 2021, 11, 705–725.
- [41] Z. Li, Z. An, Y. Guo, K. Zhang, X. Chen, D. Zhang, Z. Xue, X. Zhou, X. Lu, *Talanta* **2016**, *161*, 713–720.
- [42] N. Bommireddy, S. K. Palathedath, J. Electroanal. Chem. **2020**, 856, 113660.
- [43] P. Lei, Y. Zhou, R. Zhu, S. Wu, C. Jiang, C. Dong, Y. Liu, S. Shuang, *Microchim. Acta* **2020**, *187*, 1–9.
- [44] F. Xia, B. Li, Y. Liu, H. Tan, B. An, S. Gao, T. J. Marks, Y. Cheng, *Adv. Funct. Mater.* **2024**, *34*, 2312079.
- [45] W. Gao, K. Xie, J. Xie, X. Wang, H. Zhang, S. Chen, H. Wang, Z. Li, C. Li, *Adv. Mater.* **2023**, *35*, 2202952.
- [46] Z. Mumtarin, M. M. Rahman, H. M. Marwani, M. A. Hasnat, *Electrochim. Acta* **2020**, 346, 135994.
- [47] M. N. Islam, M. Ahsan, K. Aoki, Y. Nagao, A. E. Alsafrani, H. M. Marwani, A. Almahri, M. M. Rahman, M. A. Hasnat, *J. Environ. Chem. Eng.* **2023**, *11*, 111149.
- [48] H. Begum, M. N. Islam, S. Ben Aoun, J. A. Safwan, S. S. Shah, M. A. Aziz, M. A. Hasnat, *Environ. Sci. Pollut. Res.* **2023**, *30*, 34904–34914.
- [49] M. A. Hasnat, M. A. Rashed, S. Ben Aoun, S. M. N. Uddin, M. S. Alam, S. Amertharaj,

- R. K. Majumder, N. Mohamed, J. Mol. Catal. A Chem. 2014, 383, 243–248.
- [50] F. Islam, M. Ahsan, N. Islam, M. I. Hossain, N. M. Bahadur, A. Aziz, J. Y. Al-Humaidi, M. M. Rahman, T. Maiyalagan, M. A. Hasnat, *Chem. An Asian J.* **2024**, e202400220.
- [51] K. Uosaki, G. Elumalai, H. C. Dinh, A. Lyalin, T. Taketsugu, H. Noguchi, *Sci. Rep.* **2016**, 6, 32217.
- [52] S. Shin, Z. Jin, D. H. Kwon, R. Bose, Y.-S. Min, *Langmuir* **2015**, *31*, 1196–1202.
- [53] A. Yasir Abir, S. M. Nizam Uddin, M. Hasan, M. Abdul Aziz, S. Shah, J. Ahmed, M. Abul Hasnat, *Results Chem.* **2023**, *5*, 100702.
- [54] Z. Z. Tasic, M. M. Antonijevic, *Chem. Pap.* **2016**, *70*, 620–634.
- [55] V. Thaçi, R. Hoti, A. Berisha, J. Bogdanov, Open Chem. 2020, 18, 1412–1420.
- [56] N. H. Turner, A. M. Single, Surf. Interface Anal. 1990, 15, 215–222.
- [57] V. Krylova, M. Andrulevičius, Int. J. Photoenergy 2009, 2009, 1–8.
- [58] D. Briggs, *Handbook of X-Ray Photoelectron Spectroscopy*, John Wiley & Sons, Ltd, **1981**.
- [59] S. Krishnamurthy, A. Esterle, N. C. Sharma, S. V Sahi, *Nanoscale Res. Lett.* **2014**, *9*, 1–9.
- [60] R. Betancourt-Galindo, P. Y. Reyes-Rodriguez, B. A. Puente-Urbina, C. A. Avila-Orta, O. S. Rodríguez-Fernández, G. Cadenas-Pliego, R. H. Lira-Saldivar, L. A. García-Cerda, *J. Nanomater.* **2014**, *2014*, 980545.
- [61] Y. Fu, R. Yuan, L. Xu, Y. Chai, Y. Liu, D. Tang, Y. Zhang, *J. Biochem. Biophys. Methods* **2005**, *62*, 163–174.
- [62] M. Duca, V. Kavvadia, P. Rodriguez, S. C. S. Lai, T. Hoogenboom, M. T. M. Koper, *J. Electroanal. Chem.* **2010**, *649*, 59–68.
- [63] A. C. A. De Vooys, G. L. Beltramo, B. Van Riet, J. A. R. Van Veen, M. T. M. Koper, *Electrochim. Acta* **2004**, *49*, 1307–1314.
- [64] J. Baltrusaitis, P. M. Jayaweera, V. H. Grassian, *Phys. Chem. Chem. Phys.* **2009**, *11*, 8295–8305.
- [65] I. Louis-Rose, C. Méthivier, J. C. Védrine, C.-M. Pradier, *Appl. Catal. B Environ.* **2006**, 62, 1–11.
- [66] A. Galtayries, E. Laksono, J. Siffre, C. Argile, P. Marcus, *Surf. Interface Anal.* **2000**, *30*, 140–144.
- [67] D. Pletcher, R. Greff, R. Peat, L. M. Peter, J. Robinson, *Instrumental Methods in Electrochemistry*, Elsevier, **2001**.
- [68] A. J. Bard, L. R. Faulkner, H. S. White, *Electrochemical Methods: Fundamentals and Applications*, John Wiley & Sons, **2022**.
- [69] A. Muthukrishnan, V. Boyarskiy, M. V. Sangaranarayanan, I. Boyarskaya, *J. Phys. Chem. C* **2012**, *116*, 655–664.
- [70] E. Andreoli, V. Annibaldi, D. A. Rooney, K. Liao, N. J. Alley, S. A. Curran, C. B. Breslin, *Electroanalysis* **2011**, *23*, 2164–2173.
- [71] F. Manea, A. Remes, C. Radovan, R. Pode, S. Picken, J. Schoonman, *Talanta* **2010**, *83*, 66–71.
- [72] N. Comisso, S. Cattarin, P. Guerriero, L. Mattarozzi, M. Musiani, L. Vázquez-Gómez, E. Verlato, *J. Solid State Electrochem.* **2016**, *20*, 1139–1148.
- [73] D. Chen Legrand, C. Barus, V. Garcon, *Electroanalysis* **2017**, *29*, 2882–2887.
- [74] E. Lebon, P. Fau, M. Comtat, M. L. Kahn, A. Sournia-Saquet, P. Temple-Boyer, B. Dubreuil, P. Behra, K. Fajerwerg, *Chemosensors* **2018**, *6*, 50.
- [75] B. Hafezi, M. R. Majidi, *Anal. methods* **2013**, *5*, 3552–3556.

[76] L. Yu, Q. Zhang, Q. Xu, D. Jin, G. Jin, K. Li, X. Hu, Talanta 2015, 143, 245–253.

Graphical Abstract



A Cu-modified Au electrode was employed for electrocatalytic NO_3^- reduction under N_2 , O_2 , and CO_2 gas environments. N_2 showed no interference, while O_2 caused some hindrance during NRR. Notably, NRR was catalytically more efficient in the presence of CO_2 , due to the neutralization of the NRR byproduct OH^- by CO_2 gas molecules.